ARTICLE

Orthogonal Reactivity of Metal and Multimetal Nanostructures for Selective, Stepwise, and Spatially-Controlled Solid-State Modification

Brian M. Leonard, Mary E. Anderson, Karl D. Oyler, Ting-Hao Phan, and Raymond E. Schaak*

Department of Chemistry and Materials Research Institute, The Pennsylvania State University, University Park, Pennsylvania 16802

ABSTRACT Chemists rely on a toolbox of robust chemical transformations for selectively modifying molecules with spatial and functional precision to make them more complex in a controllable and predictable manner. This manuscript describes proof-of-principle experiments for a conceptually analogous strategy involving the selective, stepwise, and spatially controlled modification of inorganic nanostructures. The key concept is orthogonal reactivity: one component of a multicomponent system reacts with a particular reagent under a specific set of conditions while the others do not, even though they are all present together in the same reaction vessel. Using the chemical conversion of metal nanoparticles into intermetallic, sulfide, and phosphide nanoparticles as representative examples, the concept of orthogonal reactivity is defined and demonstrated for a variety of two- and three-component nanoscale systems. First, solution-phase reactivity data are presented and collectively analyzed for the reaction of metal nanoparticles (Ni, Cu, Rh, Pd, Ag, Pt, Au, Sn) with several metal salt and elemental reagents (Bi, Pb, Sb, Sn, S). From these data, several two- and three-component orthogonal systems are identified. Finally, these results are applied to the spatially selective chemical modification of lithographically patterned surfaces and striped template-grown metal nanowires.

KEYWORDS: metal nanoparticles · intermetallic nanoparticles · synthesis · orthogonal reactivity · metal nanowires · patterned surfaces

Chemists are able to construct complex molecules in a stepwise and predictable manner by carrying out textbook-style reactions that link together, split apart, or selectively modify simple molecular building blocks. Collectively, these synthetic capabilities form the cornerstone of molecular chemistry and allow routine access to complex molecules that contain a variety of chemically distinct functionalities within a single molecule. For example, one can react and assemble molecules to form almost countless arrangements, including derivative molecules, macromolecules, natural products, and polymers, using well-established and ever-growing libraries of chemical transformations.[1−3] To accomplish this, one part of a multifunctional molecule can be modified using chemical reactions that are selective to that functionality in the presence of others. The basis for this is orthogonal reactivity—the idea that different functionalities react differently under the same conditions (*e.g.*, one reacts and the others do not), and different conditions are required for all components to react. Put another way, in a one-pot reaction, conditions can be found to selectively react one component of a molecule while leaving the others untouched, followed by the reaction of another component in a subsequent step.

Interfacing these ideas from molecular chemistry with demands and challenges from nanoscience could lead to more advanced nanoscale architectures than are currently achievable, as well as open new doors for designing and programming the synthesis of complex nanomaterials. As an example, it is straightforward to synthesize a variety of multisegment metal nanowires, such as Au−Ag−Au or Pt−Ni−Pt, using template-confined electrodeposition.[4−8] However, methods for synthesizing analogous multisegment nanowires that incorporate stoichiometrically controllable multielement components (*e.g.*, alloys, intermetallics, metal sulfides, mixed metal oxides, *etc.*) exist in some cases but are not always generally applicable and must be approached on a case-by-case basis.[9−11] Other classes of heterostructured nanoscale materials, including nanoparticle dimers and trimers,[12−20] capped nanorods,[21−25] and core−shell nanocrystals,[26−29] are also limited in the complexity of solids that are routinely incorporated into them. It is therefore desirable to develop robust and materials-general strategies that bridge the gap between current synthetic capabilities that are simple and mature and those that are desired, but

*Address correspondence to schaak@chem.psu.edu.

Received for review December 23, 2008 and accepted February 16, 2009.

Published online February 25, 2009.
10.1021/nn800892a CCC: $40.75

are more challenging. The goal is to produce a reaction paradigm for nanoscale solids that mimics the toolbox of textbook-style reactions available to molecular chemists for transforming simple molecular building blocks into more complex molecules using reliable, reproducible, and straightforward reactions, for example, a "total synthesis" approach to the selective solid-state modification of multicomponent nanostructures.

Toward that goal, we set out to apply the idea of orthogonal reactivity to metal nanoparticle systems. This approach exploits the idea of "conversion chemistry" that we and others are developing for the chemical transformation of one type of nanoparticle into another.[30−42] Importantly, these conversion reactions often proceed with morphological retention, generating shape-controlled nanocrystals in multielement systems where composition is also controlled. For example, shape-controlled single-metal nanoparticles that are straightforward to synthesize (*e.g.*, noble metals) can be converted into derivative nanoparticles of metal sulfides,[43] metal oxides,[44,45] metal phosphides,[38] and intermetallic compounds.[31] To accomplish these chemical transformations of nanoparticles, appropriate conditions must be found to facilitate the reactions. In some cases, reactions can occur at room temperature, for instance, the reaction of cobalt with sulfur to form Co_3S_4.[43] In other cases, higher temperatures (>350 °C) are needed, for instance, the reaction of cobalt with trioctylphosphine (TOP) to form CoP.[37] Other examples at intermediate temperatures are also known. When these synthetic conditions are collectively analyzed, it becomes evident that for a given metal, chemical transformations occur with different reactants at different temperatures, but often under otherwise similar conditions (*e.g*, solvent, atmosphere, reaction time), as mentioned for the cobalt system above. Likewise, under identical reaction conditions, some metals will react with a reagent and others will not. For example, if Ni and Co nanoparticles are reacted with TOP at 300 °C, Ni will form Ni_2P, but Co will not react. Only after heating above 350 °C will the Co react to form CoP.[37]

These differences in reactivity for different metals under different conditions are certainly not surprising, as this is a central component of inorganic chemistry. However, it is the collective analysis and application of this data that is important for advancing the synthesis of inorganic nanomaterials. Indeed, these are simple examples of orthogonal reactivity, a metal nanoparticle analogy to orthogonal reactions used extensively in molecular chemistry. If this idea could be expanded and generalized to many different types of metal nanoparticle systems and reagents, it would be possible to develop a robust toolbox of orthogonal chemical transformations for selectively converting one metal into a derivative compound in the presence of other metals and/or reagents. If such chemistry were then compatible with chemical transformations of segmented

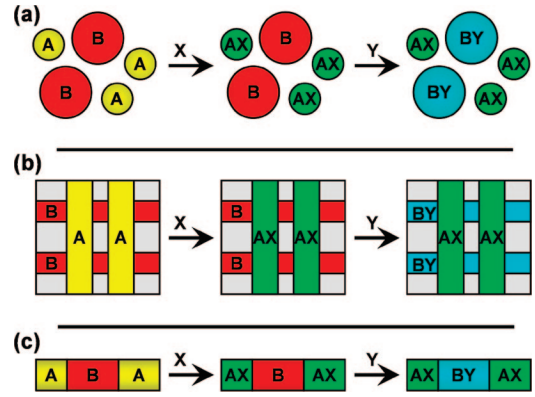

Scheme 1. Three applications of orthogonal reactivity outlined for different metal nanostructures. (a) Reagent X is added to a mixture of two different types of metal nanoparticles, A and B, in a single pot. The reaction is selective for A, forming AX but leaving B unreacted. Reagent Y is then added, which selectively reacts with B to form BY but is unreactive toward AX. (b) Similar reactivity sequence, but involving metals A and B deposited as a patterned planar film and the reactions carried out on the surface-confined nanostructures. (c) Similar reactivity sequence, but applied to A−B−A striped metal nanowires, using orthogonal reactivity to selectively react the tips (A → AX) first, followed by the center (B → BY).

nanowires and heterostructured nanoparticles, for example, truly selective orthogonal conversions could be carried out in a spatially controllable manner in order to generate exceptionally complex multicomponent nanostructures in an on-demand and by-design fashion. Since the products of many of these chemical transformations maintain the morphology of the metal nanoparticle precursors, often involving single-crystal transformations, it is reasonable to anticipate the successful application of these ideas to heterostructured nanoscale systems without destroying the morphology, providing that interfacial stability can be retained.

Here we establish the concept of orthogonal reactivity for metal nanoparticle systems based on the idea of converting metal nanoparticle precursors into derivative multielement intermetallic, sulfide, and phosphide nanoparticles. We study and define the conditions under which an extensive library of chemical transformations occur and demonstrate that multiple reactions can be carried out in sequence in a one-pot reaction, which is central to the idea of orthogonal reactivity. As a result of these studies, we also report the formation of several intermetallic compounds that are known but have not been previously reported as polyol-derived nanocrystals. Finally, we apply the concept of orthogonal reactivity to lithographically patterned surfaces and template-grown striped metal nanowires as representative examples of its utility in generating complex spatially defined nanoscale heterostructures.

RESULTS AND DISCUSSION

The concept of orthogonal reactivity as applied to the chemical conversion of metal nanoparticles into intermetallic compounds is shown in Scheme 1a. Briefly,

TABLE 1. Details for the Synthesis of Binary Intermetallics Using Metal Nanoparticle Precursors[a]

Metal NP	$Bi(NO_3)_3$	$Pb(C_2H_3O_2)_2$	$SbCl_3$	$SnCl_2$	S
Ni	NiBi (220 °C)	N.R.	NiSb (25 °C)	Ni_3Sn_4 (100 °C)	M.P.
Cu	N.R.	N.R.	Cu_2Sb (250 °C)	Cu_6Sn_5 (120 °C)	Cu_2S
Rh	RhBi (200 °C)	M.P.	RhSb (180 °C)	$RhSn_2$ (240 °C)	N.R.
Pd	β-PdBi (240 °C)	Pd_5Pb_3 (120 °C)	Pd_8Sb_3 (200 °C)	$PdSn_2$ (200 °C)	M.P.
Ag	N.R.	N.R.	Ag_3Sb (280 °C)	Ag_4Sn (175 °C)	Ag_2S
Pt	PtBi (230 °C)	PtPb (150 °C)	PtSb (200 °C)	PtSn (200 °C)	PtS_2
Au	N.R.	N.R.	N.R.	AuSn (25 °C)	N.R.[b]
Sn	N.R.	N.R.	SnSb (150 °C)	Sn	SnS

[a] $NaBH_4$ solution was added after the metal salt solution for each of the reactions. N.R. means that no reaction was observed by powder X-ray diffraction for the precipitated powder. M.P. means that reactions produced crystalline mixed-phase products. [b] Reactions between Au and S will block the surface of Au prohibiting further reactions but no Au−S phases form.

preformed metal nanoparticles are reacted with metal salt solutions under reducing conditions, and the choice of temperature and other reaction conditions determines whether a particular metal nanoparticle will or will not react. In this way, multiple types of nanoparticles can be converted, in a sequential and stepwise manner, into multiple distinct products in a one-pot reaction. A similar concept can be envisioned for spatially defined nanostructures, for example, lithographically patterned surfaces (Scheme 1b) and striped template-grown metal nanowires (Scheme 1c). To realize this concept of orthogonal reactivity, we first (a) establish the conditions necessary to carry out solution-mediated metal to intermetallic conversions in a number of nanoparticle systems, (b) identify systems that exhibit orthogonal reactivity, and (c) apply the orthogonal reactions to multicomponent spatially defined nanostructures.

Establishing Orthogonal Reactivity for Metal Nanoparticles. Nanoparticles of Ni, Cu, Rh, Pd, Ag, Pt, Au, and Sn were synthesized by borohydride reduction of soluble metal salt precursors in tetraethylene glycol (TEG) (Supporting Information, Figure S1). No effort was taken to control nanoparticle shape and size, since it was not necessary for determining optimal reaction conditions. However, all particles were typically in the range of 5−25 nm, as observed by TEM. These preformed metal nanoparticles were then reacted with stoichiometric amounts of metal salt solutions under reducing conditions to establish temperature-dependent reactivity in each system. The binary systems were chosen to represent a range of physical properties and potential applications (magnetic, superconducting, catalytic, thermoelectric, energy storage, semiconductors, *etc.*). Representative XRD data for aliquots taken at various temperatures in the Ni−Sn system (Figure S2) show the onset of crystallization of Ni_3Sn_4 around 100 °C. Accordingly, this is considered, for the purposes of this study, to be the lowest optimal temperature for forming Ni_3Sn_4 by reacting Ni nanoparticles with a TEG solution of $SnCl_2$. Similar aliquot experiments were performed for all of the (Ni, Cu, Rh, Pd, Ag, Pt, Au, Sn)−(Bi, Pb, Sb, Sn, S) binary systems, and the temperature-dependent reactivity data are compiled in Table 1. (Note that, for purposes of comparison, these temperatures were determined using otherwise similar conditions for all systems. For systems where reactivity has occurred but products are mixed-phase, it is reasonable to anticipate that additional optimization of conditions could lead to phase-pure products. Conditions may also need to be modified for systems with larger feature sizes.) Also included in Table 1 are several nanocrystalline intermetallic compounds that have not previously been reported as products of polyol reactions. Specifically, RhSb, RhBi, PdBi, Pd_8Sb_3, and Pd_5Pb_3 are known in bulk systems and many have useful catalytic properties, but have not previously been reported as nanocrystals using low-temperature solution routes.

Inspection of the data in Table 1 shows that some intermetallics form under similar conditions (*e.g.*, NiBi, RhBi, Pd_8Sb_3, PtSb, $PdSn_2$, PtSn, *etc.*), and as a result, these systems would not exhibit orthogonal reactivity. However, a number of other metal nanoparticle systems form intermetallic products under very different conditions (*e.g.*, NiBi/NiSb/Ni_3Sn_4, PdBi/Pd_5Pb_3/Pd_8Sb_3, Ag_4Sn/Ag_2S, PtBi/PtPb/PtSb), and these would be expected to show orthogonal reactivity. Similarly, Table 1 indicates that orthogonal reactions of multiple types of nanoparticles with the same metal salt solution are possible. For example, many of the metal nanoparticles studied react with Sn, but at notably different temperatures: AuSn forms near room temperature, Ni_3Sn_4 forms at 100 °C, Ag_4Sn forms at 175 °C, and $PdSn_2$ and PtSn form at 200 °C. Thus, guided by the lowest temperature where a particular intermetallic phase forms, it should be possible to react one type of metal nanoparticle while leaving another metal nanoparticle in the same solution unreacted, consistent with the concept of orthogonal reactivity.

Figure 1 shows XRD data demonstrating the concept of orthogonal reactivity. Nanoparticles of β-Sn, Pt, and Ag are reacted in TEG (in separate reaction flasks) sequentially with $FeCl_3$ at 170 °C, $SbCl_3$ at 200 °C, and

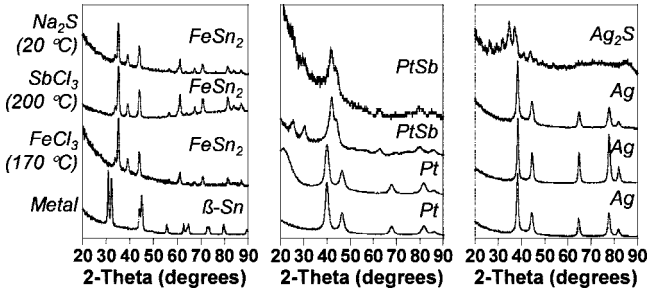

Figure 1. Powder XRD data highlighting three-component orthogonal reactivity in the (Sn,Pt,Ag)−(Fe,Sb,S) systems. When $FeCl_3$ is added to a TEG solution of β-Sn nanoparticles and heated to 170 °C, $FeSn_2$ forms. When $FeCl_3$ is added to TEG solutions of Pt and Ag and heated to 170 °C, no reactions occur. $FeSn_2$ and Ag do not react with $SbCl_3$ at 200 °C, but Pt does, forming PtSb. PtSb and $FeSn_2$ do not react with Na_2S at 20 °C, but Ag does, forming Ag_2S.

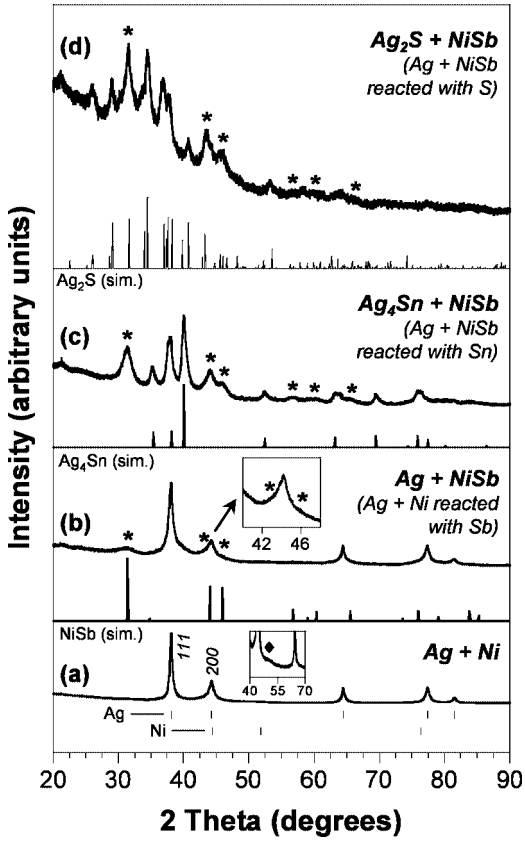

Figure 2. Powder XRD data demonstrating one-pot two-component orthogonal reactivity in the (Ag,Ni)−(Sb,Sn,S) systems. A mixture of Ag and Ni nanoparticles (a) are reacted with $SbCl_3$ at 100 °C to form NiSb (b), leaving the Ag unreacted. [The inset in panel a shows the broad *200* reflection for Ni. The inset in panel b shows two NiSb peaks as broad shoulders on either side of the Ag *200* peak.] The mixture of Ag and NiSb nanoparticles is then reacted with $SnCl_2$ at 175 °C to form Ag_4Sn (c). The NiSb persists, changing only in its crystallinity because of the additional heating time. The Ag in the Ag−NiSb mixture can also be selectively reacted with Na_2S at room temperature to form Ag_2S (d), leaving the NiSb unreacted. The asterisks in (b), (c), and (d) correspond to the most prominent NiSb peaks. Other simulated XRD patterns are shown below the experimental data.

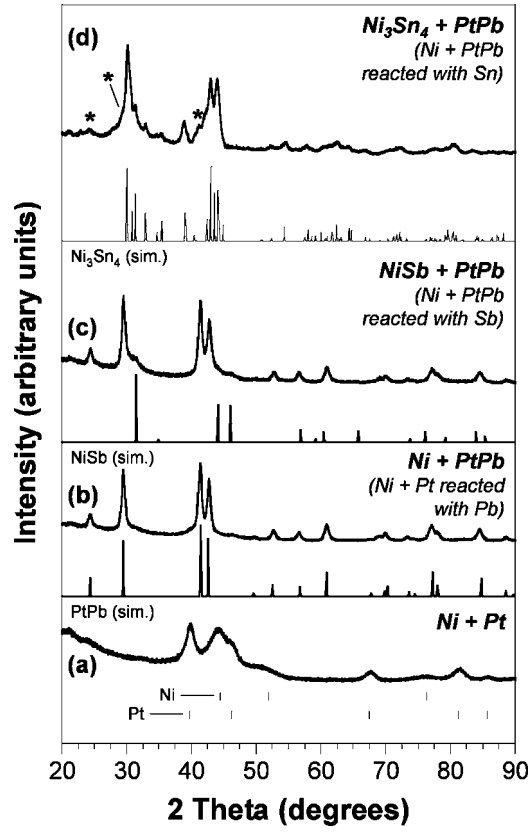

Figure 3. Powder XRD data demonstrating one-pot two-component orthogonal reactivity in the (Ni,Pt)-(Pb,Sb,Sn) systems. A mixture of Ni and Pt nanoparticles (a) are reacted with $Pb(C_2H_3O_2)_2$ at 150 °C to form PtPb (b), leaving the Ni unreacted. [The nanocrystalline Ni appears as a broad feature near 45 °2θ.] The mixture of Ni and PtPb nanoparticles is then reacted with $SbCl_3$ at 100 °C to form NiSb (c), with the PtPb remaining unchanged. The Ni in the Ni−PtPb mixture can also be selectively reacted with $SnCl_2$ at 120 °C to form Ni_3Sn_4 (d), with the PtPb persisting through the reaction. The asterisks in panel d correspond to the most prominent peaks for PtPb.

Na_2S at 20 °C. When Sn is reacted with $FeCl_3$ at 150−170 °C, $FeSn_2$ forms. In contrast, Ag and Pt do not react with Fe under these conditions. When $FeSn_2$, Ag, and Pt are separately reacted with $SbCl_3$ at 200 °C, PtSb forms, but no Ag−Sb phase forms, nor does $FeSn_2$ react. When Ag, $FeSn_2$, and PtSb react with Na_2S at 20 °C, Ag converts to Ag_2S, but $FeSn_2$ and PtSb remain nominally unchanged. Thus, the orthogonal reactivity is such that Sn, Pt, and Ag nanoparticles can be sequentially converted to $FeSn_2$, PtSb, and Ag_2S.

The above example demonstrates chemistry that supports three-component orthogonal reactivity, but not in a single one-pot reaction. Figure 2 shows XRD data that demonstrates true two-component orthogonal reactivity in a single pot. Ag and Ni nanoparticles are mixed in a single reaction flask, and the XRD data shows primarily Ag along with broad peaks that correspond to Ni (Figure 2a). Note that the Ni particles are multidomain and smaller than the Ag, making the Ni phase difficult to detect. The inset to Figure 2a shows an enlarged version of the XRD data, confirming the presence of Ni. When $SbCl_3$ is added to the mixture of Ag and Ni nanoparticles and reacted at 100 °C, NiSb forms, but the Ag remains unreacted (Figure 2b). A simulated XRD pattern for NiSb is shown below the experimental data. The primary reflection for NiSb can be seen as a broad peak at 31.5 °2θ, and the peaks around 44 and 46 °2θ are evident as small shoulders on the Ag *200* peak. When the mixture of Ag and NiSb nanoparticles is reacted with $SnCl_2$ at 175 °C, the Ag forms Ag_4Sn while the NiSb remains unreacted (Figure 2c). The NiSb has been further crystallized and the Ag reacted to form Ag_4Sn in Figure 2c, making the NiSb phase clearly evident by XRD. Instead of reacting NiSb and Ag with $SnCl_2$, they can instead be reacted with sulfur at room temperature for 4 h to convert the Ag to Ag_2S while leaving the NiSb largely unchanged (Figure 2d).

Figure 3 shows another two-component one-pot orthogonal system. Ni and Pt nanoparticles (Figure 3a)

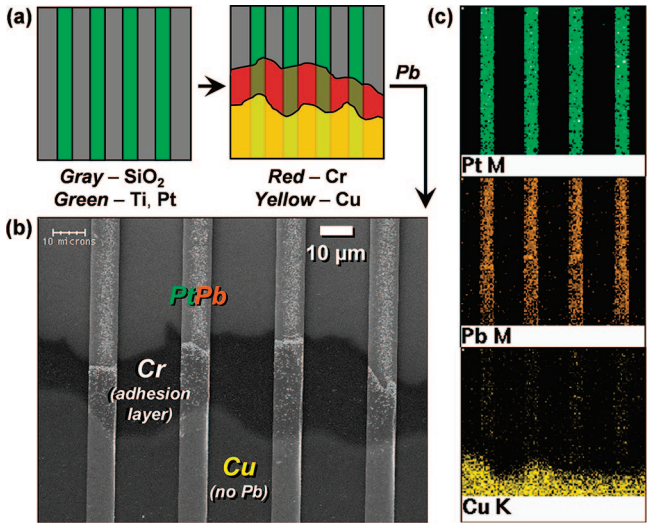

Figure 4. (a) Schematic of the steps involved in lithographically fabricating the patterned test sample with discrete areas of Pt and Cu metal: Pt stripes (with Ti adhesion layer) were lithographically patterned onto a silicon substrate, then an irregularly shaped Cu region (with Cr adhesion layer) was patterned using a hard shadow mask. For characterizing the patterned surface after reacting with $Pb(C_2H_3O_2)_2$ at 150 °C, SEM (b) and associated EDS element mapping (c) data verify that the Pt stripes reacted with the Pb to form PtPb stripes, while the Cu did not react (no Pb is present in the Cu region).

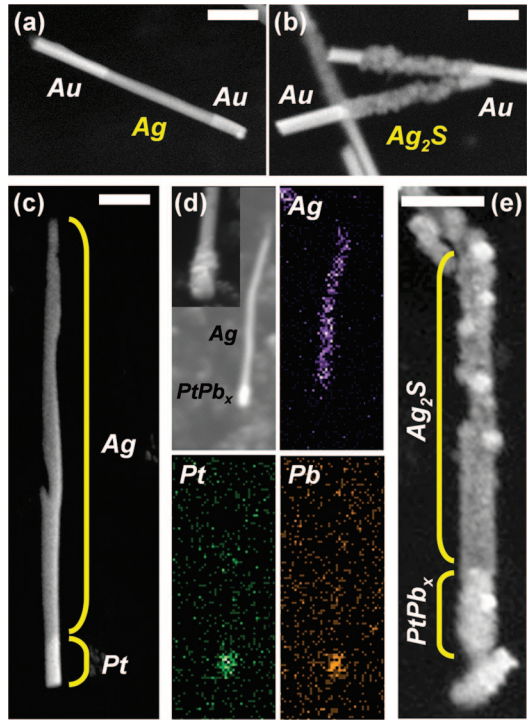

Figure 5. SEM images of a (a) Au−Ag−Au nanowire and (b) Au−Ag_2S−Au nanowires formed after a site-specific orthogonal reaction with sulfur at room temperature. SEM images of (c) as-deposited Ag−Pt nanowire, (d) after selectively converting the Pt tip to $PtPb_x$ (with element maps for Ag, Pt, and Pb showing the incorporation of Pb only on the Pt tips), and (e) after selectively converting the Ag section to Ag_2S. [Ag and S have overlapping EDS peaks so element mapping is not instructive, but the reactivity can be inferred *via* the roughened morphology.] All scale bars represent 1 µm.

are reacted with $Pb(C_2H_3O_2)_2$ at 150 °C to form PtPb (Figure 3b), while Ni remains unreacted (appears as very broad peaks that are difficult to distinguish in the presence of the sharper PtPb peaks). Subsequently, $SbCl_3$ is added to the mixture of Ni and PtPb nanoparticles and reacted at 100 °C to form NiSb and PtPb (Figure 3c). Instead of reacting with $SbCl_3$ in the final step, the Ni and PtPb can be reacted with $SnCl_2$ at 120 °C to form Ni_3Sn_4 and PtPb (Figure 3d).

Applying Orthogonal Reactivity to Spatially-Defined Nanostructures. The experiments described above clearly define the conditions under which various metal-to-intermetallic conversions occur, and also demonstrate true orthogonal reactivity in several systems. However, the power of orthogonal reactivity is its potential ability to be applied to spatially defined nanostructures, where prepatterned materials can be sequentially reacted to achieve both compositional and spatial control over multiple multielement phases, which would otherwise be difficult or impossible to achieve.

Figure 4 shows a simple proof-of-concept example of orthogonal reactivity applied to lithographically patterned surfaces. Figure 4a shows a schematic of the test sample that contains vertical Pt stripes and irregularly shaped Cu pads. The Pt features were patterned first *via* photolithography and evaporation of 10 nm Ti and 90 nm Pt. The Cu pads were then patterned using a hard shadow mask, with evaporation of a 10 nm Cr adhesion layer and 90 nm of Cu. This surface patterned with microscale Pt and Cu features was immersed in a TEG solution of $Pb(C_2H_3O_2)_2$ and heated to 150 °C. According to Table 1, Pt should react with the Pb salt solution at 150 °C to form PtPb. However, Cu should not react with Pb at any temperature obtainable in TEG. Thus, one would predict that the simultaneous reaction of Pt and Cu in $Pb(C_2H_3O_2)_2$ at 150 °C should generate PtPb and Cu without forming any undesired Cu−Pb phases. The SEM and EDS element mapping data in Figure 4b,c show that this is indeed the case: the Pb is present only where there is Pt, indicating that Pb reacted only with the Pt to form patterned stripes of PtPb; the Cu did not react. This represents the application of orthogonal reactivity to lithographically patterned substrates, and could be useful for the *in situ* modification of materials being interrogated by electrodes without modifying the electrodes themselves.

Multisegment template-grown metal nanowires are another application of orthogonal reactivity to patterned nanostructures, as shown in Figure 5. A three-segment Au−Ag−Au nanowire (Figure 5a) can be reacted with sulfur in TEG at room temperature to form Au−Ag_2S−Au striped nanowires (Figure 5b). A further demonstration of this orthogonal reactivity is shown in Figure 5c for Ag nanowires with Pt tips. Table 1 suggests that when a mixture of Ag and Pt is reacted with $Pb(C_2H_3O_2)_2$ above 150 °C, the Pt will form PtPb, but the Ag will remain unreacted. Accordingly, the SEM micrograph and EDS mapping data in Figure 5d confirm that

after releasing the Ag−Pt nanowires from the membranes and reacting them with $Pb(C_2H_3O_2)_2$ in TEG at 200 °C, the Pb reacts only with the Pt tip. The result is a Ag−$PtPb_x$ two-segment metal−intermetallic nanowire. XRD data for this sample (Supporting Information) confirm that all of the Pt has reacted, forming a mixture of PtPb and $PtPb_4$. This phase mixture is likely to result from minor diffusion limitations, with a hypothesized Pb-rich shell, in analogy to the result of other similar diffusion-based reactions on larger nano- and microstructures.[37] Likewise, after reacting the Ag−$PtPb_x$ nanowire with sulfur in TEG at room temperature, the Ag selectively reacts to form Ag_2S while the $PtPb_x$ remains unchanged. This is also confirmed by the XRD data in Supporting Information. The result, shown in Figure 5e, is a two-segment chalcogenide-intermetallic (Ag_2S−$PtPb_x$) nanowire that is formed by applying the concept of orthogonal reactivity to patterned metal nanowire systems.

Similar orthogonal-mediated transformations can generate other types of striped metal nanowires and can be performed while the electrodeposited nanowires are maintained within their template membrane.[46] For example, membrane-bound Pt−Ni two-segment nanowires (Figure 6a) were partially reacted with TOP at 330 °C to form Pt−Ni−Ni_2P nanowires. This was done with the Ag backing intact on the membrane to help protect the Pt nanowire tips from reacting with TOP. (Pt reacts with TOP at 370 °C to form PtP_2, so physical protection, *e.g.*, the Ag backing electrode acting as a type of protecting group, can help to mediate situations where multiple regions would be reactive under the same conditions.) This is followed by removal of the Ag film and subsequent partial reaction with $Pb(C_2H_3O_2)_2$ at 200 °C to form PtPb−Pt−Ni−Ni_2P intermetallic−metal−phosphide striped nanowires (Figure 6b,c). XRD data (not shown) confirm the formation of PtPb, Pt, Ni, and Ni_2P with no Pt−P or Ni−Pb phases present. The extent to which the nanowire is converted is dependent on the solution conditions as previously demonstrated,[46] allowing the stripe dimensions of the nanowire to be tailored.

Image contrast and nanowire morphology *via* SEM provide some evidence of the spatially defined chemical conversion, as does spatially resolved EDS data. EDS spectra collected from the PtPb tips (Figure 6d) verify the presence of Pt and Pb, while the EDS spectra collected from the Ni_2P tips (Figure 6f) verify the presence of Ni and P and the absence of Pt and Pb. EDS spectra collected at the Pt/Ni interface verify the absence of P and Pb in this interfacial region (Figure 6e). Taken together, the data are consistent with a PtPb−Pt−Ni−Ni_2P four-segment nanowire formed by applying the concept of orthogonal reactivity to the spatially selective modification of template-grown metal nanowires.

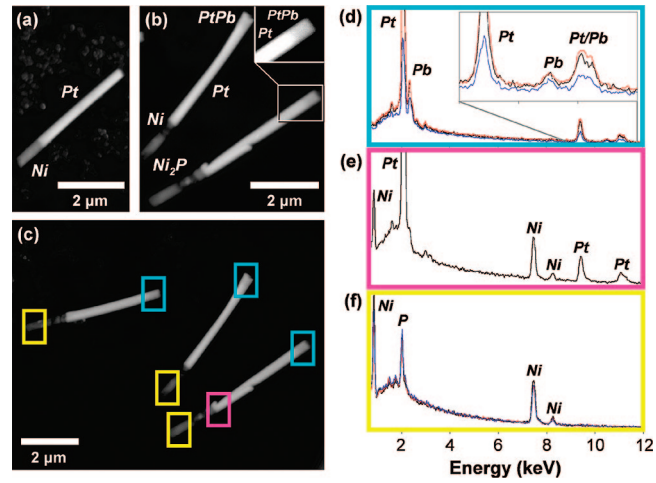

Figure 6. SEM images of (a) two-segment Pt−Ni nanowires and (b) four-segment Ni_2P−Ni−Pt−PtPb nanowires after sequential reactions on each of the tips. The different regions can be seen through contrast differences (*e.g.*, the PtPb-Pt tip, which has been enlarged and contrast-enhanced in the inset). EDS spectra (d−f) were collected at the nanowire sections indicated in the SEM image in panel c. The blue boxes around the PtPb tips correspond to the EDS spectra in panel d, showing an enlargement of the L-lines in the inset. This shows that both Pt and Pb are present. The yellow boxes around the Ni_2P tips in panel c, which correspond to the EDS spectra in panel f, confirm that both Ni and P are present. The spectra for all three nanowires in panel c are shown, each represented with a different color [bottom right wire, black; middle, red; top left, blue]. An EDS spectrum at the Ni/Pt interface, highlighted in pink in panel c and shown in panel e, confirms that Ni and Pt are present and that Pb is not.

CONCLUSIONS

In this paper, we developed the general concept of orthogonal reactivity as it applies to the sequential and stepwise chemical modification of metal nanoparticle systems. This synthetic framework makes it possible to merge the benefits of solution chemistry routes to nanoparticles (materials generality and easy access to multielement systems) with the benefits of other spatially controllable nanostructure fabrication methods (lithographic patterning of metals, template synthesis of striped nanowires). Application and expansion of this concept to other chemical systems and types of nanostructures has the potential to significantly advance the development of multifunctional sublithographic systems that incorporate, in a spatially well-defined manner, a variety of materials in predefined and co-located patterns.

EXPERIMENTAL SECTION

Materials. The following metal reagents were used as received: sulfur powder, Na_2S, Na_2PdCl_4, $RhCl_3$, $SnCl_2$ (anhydrous, 99% min.), $Cu(C_2H_3O_2)_2 \cdot H_2O$, $HAuCl_4 \cdot 3H_2O$ (99.99%), $AgNO_3$ (99.9+%), K_2PtCl_6 (40.11% Pt), $Ni(C_2H_3O_2)_2 \cdot xH_2O$ (99+%), $SbCl_3$ (99.9%), $Pb(C_2H_3O_2)_2 \cdot 3H_2O$, and $Bi(NO_3)_3 \cdot 5H_2O$ (Mallinckrodt Chemical Works). Sodium borohydride ($NaBH_4$) was used as a reducing agent. Poly(vinyl pyrrolidone) (PVP, MW = 40000) was used as a surface stabilizer, and the solvent for all reactions was tetraethyleneglycol (TEG, 99+%), except for phosphide systems where trioctylphosphine (TOP) was used. All chemicals were pur-

chased from Alfa Aesar unless otherwise noted. For lithographic patterning, a bilayer resist stack composed of PMGI lift-off resist (Microchem LOR-1A) and positive photoresist (Shipley 3012) were used and developed using a solution containing tetramethyl ammonium hydroxide (Shipley MF-CD-26). For nanowire electrodeposition, anodic aluminum oxide membranes (Anodisc 25, Whatman Scientific, 0.2 μm) were used as the template. Nanowires with segments of Pt, Ag, Au, or Ni were fabricated by deposition from Technic plating solutions (Pt TP RTU, Ag Cyless R RTU, Au Orotemp 24-1, and Nickel S).

Synthesis. The metal nanoparticle precursors were prepared by a modified polyol process in which an appropriate metal salt and PVP were dissolved in TEG followed by heating and reduction with $NaBH_4$. For example, $Ni(C_2H_3O_2)_2 \cdot xH_2O$ (76.5 mg, 0.425 mmol) and PVP (252 mg) were dissolved in 30 mL of TEG by sonication, then the solution was stirred vigorously while bubbling Ar through the solution for 30 min. The metal salt solution was reduced with a freshly prepared solution of $NaBH_4$ in TEG (0.5 M, 2 mL) then heated to 180 °C. The reaction solution was maintained at this temperature for 10 min then cooled to room temperature.

The metal nanoparticle precursors were individually reacted with a variety of metal salts and $NaBH_4$ followed by heating to determine the temperature at which the binary intermetallic phase forms. For example, a freshly prepared TEG solution of Ni nanoparticles was stirred under bubbling Ar for 30 min, then a TEG solution of $SbCl_3$ (0.235 M) was added. This solution was stirred for 1−2 min then reduced with $NaBH_4$ (0.5 M, 2 mL). The solution was then heated and aliquots were taken at several temperatures. The aliquots were centrifuged and washed with ethanol and acetonitrile. The resulting powders were analyzed by powder XRD to determine the phase formation and the temperature at which each phase formed.

The orthogonal reactions were performed by mixing equal molar ratios of preformed metal nanoparticles in TEG and stirring the solution under bubbling Ar for 30 min. A metal salt dissolved in TEG was added to the reaction solution and reduced with $NaBH_4$. The solution was then heated to the temperature determined by the test reactions to form the first intermetallic phase. A second metal salt was then added to the solution, reduced with $NaBH_4$, and heated to a second temperature to form the second intermetallic phase. The nanocrystalline products were precipitated from solution by centrifugation and were washed with ethanol. Acetonitrile was also added to some reaction solutions to aid in precipitation of the nanocrystalline products.

Application to Lithographically-Patterned Surfaces. The surface-bound patterned metal features were fabricated by standard photolithographic methods using a hard shadow mask. A bilayer resist stack composed of an underlying lift-off resist and photoresist (Shipley 3012) was assembled on an oxidized Si wafer. Using a contact aligner (Carl Suss MA-6) and photomask, the photoresist was exposed and the bilayer resist stack subsequently developed. The photolithography was followed by Ti and Pt metal deposition and lift-off. To generate a second set of different metal features, a hard shadow mask was used during another round of evaporation for Cr and Cu features. This mask is a metal plate with patterned openings that is placed directly on the substrate, which already contains lithographically defined metal features. Solution chemistry reactions, as described above and in the Results and Discussion, were applied to these multicomponent patterned surfaces to convert the Pt features to PtPb, without altering the Cu features.

Application to Template-Grown Metal Nanowires. Nanowires were electrodeposited following standard methods published elsewhere.[4−7] Anodic aluminum oxide (AAO) membranes were used as the template, a thin Ag film (deposited thermally and electrochemically) was utilized as the working electrode, and a Pt counter-electrode was used. Constant current electrochemical deposition was used to fabricate nanowires with diameters of ~300 nm, lengths ranging from 3 to 8 μm, and segments of Pt, Ag, Au, or Ni. After electrodeposition, the silver backing was removed by exposure to 8 M HNO_3 and the AAO membrane is dissolved in 3 M NaOH. The resulting released nanowires were washed by centrifugation and stored in ethanol. These wires were used as substrates for orthogonal chemical reactions as described below.

Au−Ag−Au Nanowires. Au−Ag−Au segmented nanowires (~1.5 μm Au, ~2 μm Ag, and ~0.5 μm Au) were released from the membrane and transferred into TEG. Then, sulfur powder was added, and the mixture was stirred under Ar overnight for ~16 h at room temperature. These resulting nanowires were washed by centrifugation and stored in ethanol.

Pt−Ag Nanowires. The stepwise conversion of released Pt−Ag nanowires to PtPb−Ag_2S serves as the first demonstration of on-wire orthogonal reactivity. Pt−Ag nanowires were fabricated by electrodeposition with ~7 μm Ag segments and ~500 nm Pt segments and released from the membrane. They were transferred into a 30 mM TEG solution of $Pb(C_2H_3O_2)_2 \cdot 3H_2O$ and ~3 mL of a 0.5 M TEG solution of $NaBH_4$ was added. This combination was stirred under Ar with heating to 190 °C for 1 h, and the product was washed by centrifugation. A portion of the product was transferred into TEG, and sulfur powder was added. This mixture was stirred under Ar for 5 h at room temperature. Finally, the resulting released nanowires were washed by centrifugation and stored in ethanol.

Pt−Ni Nanowires. Pt−Ni nanowires (~4 μm Pt and ~1 μm Ni) were fabricated by electrodeposition, and the Ag backing was not removed in order to protect the Pt terminus of the wire. This conversion reaction was done on the nanowires while they were maintained within the membrane. The nanowire-containing membrane was immersed in TOP for 2 h at 330 °C to form Ni_2P. Then the Ag backing was removed and the sample was immersed in a 60 mM TEG solution of $Pb(C_2H_3O_2)_2 \cdot 3H_2O$ for 1 h at 200 °C to form PtPb. These converted nanowires were released from the membrane by exposure to NaOH and the released nanowires were washed by centrifugation and stored in ethanol.

Characterization. Powder X-ray diffraction (XRD) data were collected using Cu Kα radiation on a Bruker GADDS three-circle X-ray diffractometer, a Huber Guinier G670 Image Plate camera with a Rigaku RU200H rotating anode X-ray generator, and a Bruker D8 Advance X-ray diffractometer with LynxEye detector. All used a Cu X-ray tube. Scanning electron microscopy (SEM), energy dispersive X-ray spectroscopy (EDS), and EDS element mapping were performed using a FEI Quanta 200 environmental SEM operating in high vacuum mode, as well as a JEOL JSM 5400 scanning electron microscope.

Acknowledgment. This work was supported by NSF (DMR-0748943), a Beckman Young Investigator Award, a Sloan Research Fellowship, a DuPont Young Professor Grant, and a Camille Dreyfus Teacher-Scholar Award. SEM was performed at the Materials Characterization Facility at the Penn State Materials Research Institute and at the Huck Institutes of the Life Sciences. The authors thank Dr. Christine Keating and her group for help with nanowire electrodeposition. The authors also acknowledge use of facilities at the PSU site of the NSF NNIN.

Supporting Information Available: Additional XRD data. This material is available free of charge *via* the Internet at http://pubs.acs.org.

REFERENCES AND NOTES

1. Kim, H.; Spivak, D. A. An Orthogonal Approach to Multifunctional Molecularly Imprinted Polymers. *Org. Lett.* **2003**, *5*, 3415–3418.
2. Gilmore, C. D.; Allan, K. M.; Stoltz, B. M. Orthogonal Synthesis of Indolines and Isoquinolines *via* Aryne Annulation. *J. Am. Chem. Soc.* **2008**, *130*, 1558–1559.
3. Tam, J. P.; Yu, Q. T.; Miao, Z. W. Orthogonal Ligation Strategies for Peptide and Protein. *Biopolymers* **1999**, *51*, 311–332.
4. Nicewarner-Pena, S. R.; Freeman, R. G.; Reiss, B. D.; He, L.; Pena, D. J.; Walton, I. D.; Cromer, R.; Keating, C. D.; Natan, M. J. Submicrometer Metallic Barcodes. *Science* **2001**, *294*, 137–141.
5. Hulteen, J. C.; Martin, C. R. A General Template-Based Method for the Preparation of Nanomaterials. *J. Mater. Chem.* **1997**, *7*, 1075–1087.

6. Kline, T. R.; Tian, M.; Wang, J.; Sen, A.; Chan, M. W. H.; Mallouk, T. E. Template-Grown Metal Nanowires. *Inorg. Chem.* **2006**, *45*, 7555–7565.
7. Hust, S. J.; Payne, E. K.; Qin, L.; Mirkin, C. A. Multisegmented One-Dimensional Nanorods Prepared by Hard-Template Synthetic Methods. *Angew. Chem., Int. Ed.* **2006**, *45*, 2672–2692.
8. Mieszawska, A. J.; Jalilian, R.; Sumanasekera, G. U.; Zamborini, F. P. The Synthesis and Fabrication of One-Dimensional Nanoscale Heterojunctions. *Small* **2007**, *3*, 722–756.
9. Huang, Y. H.; Okumura, H.; Hadjipanayis, G. C.; Weller, D. CoPt and FePt Nanowires by Electrodeposition. *J. Appl. Phys.* **2002**, *91*, 6869–6871.
10. Singh, K. V.; Martinez-Morales, A. A.; Andavan, G. T. S.; Bozhilov, K. N.; Ozkan, M. A Simple Way of Synthesizing Single-Crystalline Semiconducting Copper Sulfide Nanorods by Using Ultrasonication during Template-Assisted Electrodeposition. *Chem. Mater.* **2007**, *19*, 2446–2454.
11. Pea, D. J.; Mbindyo, J. K. N.; Carado, A. J.; Mallouk, T. E.; Keating, C. D.; Razavi, B.; Mayer, T. S. Template Growth of Photoconductive Metal−CdSe−Metal Nanowires. *J. Phys. Chem. B* **2002**, *106*, 7458–7462.
12. Gu, H.; Zheng, R.; Zhang, X.; Xu, B. Facile One-Pot Synthesis of Bifunctional Heterodimers of Nanoparticles: A Conjugate of Quantum Dot and Magnetic Nanoparticles. *J. Am. Chem. Soc.* **2004**, *126*, 5664–5665.
13. Gu, H. W.; Yang, Z. M.; Gao, J. H.; Chang, C. K.; Xu, B. Heterodimers of Nanoparticles: Formation of Liquid−Liquid Interface and Particle-Specific Surface Modification by Functional Molecules. *J. Am. Chem. Soc.* **2005**, *127*, 34–35.
14. Shi, W. L.; Zeng, H.; Sahoo, Y.; Ohulchanskyy, T. Y.; Ding, Y.; Wang, Z. L.; Swihart, M.; Prasad, P. N. A General Approach to Binary and Ternary Hybrid Nanocrystals. *Nano Lett.* **2006**, *6*, 875–881.
15. Yang, J.; Elim, H. I.; Zhang, Q.; Lee, J. Y.; Ji, W. Rational Synthesis, Self-Assembly and Optical Properties of PbS-Au Heterogeneous Nanostructures *via* Preferential Deposition. *J. Am. Chem. Soc.* **2006**, *128*, 11921–11926.
16. Choi, S.-H.; Kim, E.-G.; Hyeon, T. One-Pot Synthesis of Copper-Indium Sulfide Nanocrystal Heterostructures with Acorn, Bottle, and Larva Shapes. *J. Am. Chem. Soc.* **2006**, *128*, 2520–2521.
17. Pellegrino, T.; Fiore, A.; Carlino, E.; Giannini, C.; Cozzoli, P. D.; Ciccarella, G.; Respaud, M.; Palmirotta, L.; Cingolani, R.; Manna, L. Heterodimers Based on CoPt−Au Nanocrystals with Tunable Domain Size. *J. Am. Chem. Soc.* **2006**, *128*, 6690–6698.
18. Teranishi, T.; Saruyama, M.; Nakaya, M.; Kanehara, M. Anisotropically Phase-Segregated Pd−Co−Pd Sulfide Nanoparticles Formed by Fusing Two Co-Pd Sulfide Nanoparticles. *Angew. Chem., Int. Ed.* **2007**, *46*, 1713–1715.
19. Zanella, M.; Falqui, A.; Kudera, S.; Manna, L.; Casula, M. F.; Parak, W. J. Growth of Colloidal Nanoparticles of Group II−VI and IV−VI Semiconductors on Top of Magnetic Iron−Platinum Nanocrystals. *J. Mater. Chem.* **2008**, *18*, 4311–4317.
20. Choi, S.-H.; Na, H. B.; Park, Y. I.; An, K.; Kwon, S. G.; Jang, Y.; Park, M.; Moon, J.; Son, J. S.; Song, I. C.; Moon, W. K.; Hyeon, T. Simple and Generalized Synthesis of Oxide−Metal Heterostructured Nanoparticles and their Applications in Multimodal Biomedical Probes. *J. Am. Chem. Soc.* **2008**, *130*, 15573–15580.
21. Mokar, T.; Sztrum, C. G.; Salant, A.; Rabani, E.; Banin, U. Formation of Asymmetric One-Sided Metal-Tipped Semiconductor Nanocrystal Dots and Rods. *Nat. Mater.* **2005**, *4*, 855–863.
22. Buonsanti, R.; Grillo, V.; Carlino, E.; Giannini, C.; Curri, M. L.; Innocenti, C.; Sangregorio, C.; Achterhold, K.; Parak, F. G.; Agostiano, A.; Cozzoli, P. D. Seeded Growth of Asymmetric Binary Nanocrystals Made of a Semiconductor TiO_2 Rodlike Section and a Magnetic γ-Fe_2O_3 Spherical Domain. *J. Am. Chem. Soc.* **2006**, *128*, 16953–16970.
23. Salant, A.; Amitay-Sadovsky, E.; Banin, U. Directed Self-Assembly of Gold-Tipped CdSe Nanorods. *J. Am. Chem. Soc.* **2006**, *128*, 10006–10007.
24. Carbone, L; Kudera, S.; Giannini, C.; Ciccarella, G.; Cingolani, R.; Cozzoli, P. D.; Manna, L. Selective Reactions on the Tips of Colloidal Semiconductor Nanorods. *J. Mater. Chem.* **2006**, *16*, 3952–3956.
25. Camargo, P. H. C.; Xiong, Y.; Ji, L.; Zuo, J. M.; Xia, Y. Facile Synthesis of Tadpole-like Nanostructures Consisting of Au Heads and Pd Tails. *J. Am. Chem. Soc.* **2007**, *129*, 15452–15453.
26. Wang, L. Y.; Luo, J.; Fan, Q.; Suzuki, M.; Suzuki, I. S.; Engelhard, M. H.; Lin, Y.; Kim, N.; Wang, J. Q.; Zhong, C. J. Monodispersed Core-Shell Fe_3O_4@Au Nanoparticles. *J. Phys. Chem. B* **2005**, *109*, 21593–21601.
27. Shevchenko, E. V.; Bodnarchuk, M. I.; Kovalenko, M. V.; Talapin, D. V.; Smith, R. K.; Aloni, S.; Heiss, W.; Alivisatos, A. P. Gold/Iron Oxide Core/Hollow-Shell Nanoparticles. *Adv. Mater.* **2008**, *20*, 4323–4329.
28. Talapin, D. V.; Yu, H.; Shevchenko, E. V.; Lobo, A.; Murray, C. B. Synthesis of Colloidal PbSe/PbS Core−Shell Nanowires and PbS/Au Nanowire−Nanocrystal Heterostructures. *J. Phys. Chem. C* **2007**, *111*, 14049–14054.
29. Goebl, J. A.; Black, R. W.; Ruthussery, J.; Giblin, J.; Kosel, T. H.; Kuno, M. Solution-Based II−VI Core/Shell Nanowire Heterostructures. *J. Am. Chem. Soc.* **2008**, *130*, 14822–14833.
30. Vasquez, Y.; Henkes, A. E.; Bauer, J. C.; Schaak, R. E. Nanocrystal Conversion Chemistry: A Unified and Materials-General Strategy for the Template-Based Synthesis of Nanocrystalline Solids. *J. Solid State Chem.* **2008**, *181*, 1509–1523.
31. Chou, N. H.; Schaak, R. E. Shape-Controlled Conversion of β-Sn Nanocrystals into Intermetallic M−Sn (M = Fe, Co, Ni, Pd) Nanocrystals. *J. Am. Chem. Soc.* **2007**, *129*, 7339–7345.
32. Cable, R. E.; Schaak, R. E. Solution Synthesis of Nanocrystalline M−Zn (M = Pd, Au, Cu) Intermetallic Compounds *via* Chemical Conversion of Metal Nanoparticle Precursors. *Chem. Mater.* **2007**, *19*, 4098–4104.
33. Bauer, J. C.; Chen, X.; Liu, Q.; Phan, T.-H.; Schaak, R. E. Converting Nanocrystalline Metals into Alloys and Intermetallic Compounds for Applications in Catalysis. *J. Mater. Chem.* **2008**, *18*, 275–282.
34. Dawood, F.; Leonard, B. M.; Schaak, R. E. Oxidative Transformation of Intermetallic Nanoparticles: An Alternative Pathway to Metal/Oxide Nanocomposites, Textured Ceramics, and Nanocrystalline Multimetal Oxides. *Chem. Mater.* **2007**, *19*, 4545–4550.
35. Vasquez, Y.; Luo, Z.; Schaak, R. E. Low-Temperature Solution Synthesis of the Non-Equilibrium Ordered Intermetallic Compounds Au_3Fe, Au_3Co, and Au_3Ni as Nanocrystals. *J. Am. Chem. Soc.* **2008**, *130*, 11866–11867.
36. Henkes, A. E.; Vasquez, Y.; Schaak, R. E. Converting Metals into Phosphides: A General Strategy for the Synthesis of Metal Phosphide Nanocrystals. *J. Am. Chem. Soc.* **2007**, *129*, 1896–1897.
37. Henkes, A, E.; Schaak, R. E. Trioctylphosphine: A General Phosphorous Source for the Low-Temperature Conversion of Metals into Metal Phosphides. *Chem. Mater.* **2007**, *19*, 4234–4242.
38. Henkes, A. E.; Schaak, R. E. Template-Assisted Synthesis of Shape-Controlled Rh_2P Nanocrystals. *Inorg. Chem.* **2008**, *47*, 671–677.
39. Jeong, U.; Camargo, P. H. C.; Lee, Y. H.; Xia, Y. Chemical Transformation: A Powerful Route to Metal Chalcogenide Nanowires. *J. Mater. Chem.* **2006**, *16*, 3893–3897.
40. Yin, Y.; Rioux, R. M.; Erdonmez, C. K.; Hughes, S.; Somorjai, G. A.; Alivisatos, A. P. Nanocrystals Through the Nanoscale Kirkendall Effect. *Science* **2004**, *304*, 711–714.
41. Son, D. H.; Hughes, S. M.; Yin, Y.; Alivisatos, A. P. Cation Exchange Reactions in Ionic Nanocrystals. *Science* **2004**, *306*, 1009–1012.

42. Camargo, P. H. C.; Lee, Y. H.; Jeong, U.; Zou, Z.; Xia, Y. Cation Exchange: A Simple and Versatile Route to Inorganic Colloidal Spheres with the Same Size but Different Compositions and Properties. *Langmuir* **2007**, *23*, 2985–2992.
43. Yin, Y. D.; Erdonmez, C. K.; Cabot, A.; Hughes, S.; Alivisatos, A. P. Colloidal Synthesis of Hollow Cobalt Sulfide Nanocrystals. *Adv. Funct. Mater.* **2006**, *16*, 1389–1399.
44. Yin, M.; Wu, C.-K.; Lou, Y.; Burda, C.; Koberstein, J. T.; Zhu, Y.; O'Brien, S. Copper Oxide Nanocrystals. *J. Am. Chem. Soc.* **2005**, *127*, 9506–9511.
45. Hyeon, T.; Lee, S. S.; Park, J.; Chung, Y.; Na, H. B. Synthesis of Highly Crystalline and Monodisperse Maghemite Nanocrystallites without a Size-Selection Process. *J. Am. Chem. Soc.* **2001**, *123*, 12798–12801.
46. Anderson, M. E.; Buck, M. R.; Sines, I. T.; Oyler, K. D.; Schaak, R. E. On-Wire Conversion Chemistry: Engineering Solid-State Complexity into Striped Metal Nanowires using Solution Chemistry Reactions. *J. Am. Chem. Soc.* **2008**, *130*, 14042–14043.